

Article

Optically Coupled PtOEP and DPA Molecules Encapsulated into PLGA-Nanoparticles for Cancer Bioimaging

Olena Vepris ¹, Christina Eich ¹ , Yansong Feng ², Gastón Fuentes ^{1,3} , Hong Zhang ², Eric L. Kaijzel ¹ and Luis J. Cruz ^{1,*}

¹ Translational Nanobiomaterials and Imaging Group, Department of Radiology, C2-S-Room 187, Leiden University Medical Center, Albinusdreef 2, 2333 ZA Leiden, The Netherlands; o.vepris@lumc.nl (O.V.); c.eich@lumc.nl (C.E.); gastonfe@biomat.uh.cu (G.F.); e.l.kaijzel@lumc.nl (E.L.K.)

² Van 't Hoff Institute for Molecular Sciences, University of Amsterdam, Science Park 904, 1098 XH Amsterdam, The Netherlands; fengyansong@bit.edu.cn (Y.F.); h.zhang@uva.nl (H.Z.)

³ Department of Ceramic and Metallic Biomaterials, Biomaterials Center, University of Havana, Ave Universidad e/G y Ronda, Vedado, Plaza, La Habana 10400, Cuba

* Correspondence: l.j.cruz_ricondo@lumc.nl

Abstract: Triplet-triplet annihilation upconversion (TTA-UC) nanoparticles (NPs) have emerged as imaging probes and therapeutic probes in recent years due to their excellent optical properties. In contrast to lanthanide ion-doped inorganic materials, highly efficient TTA-UC can be generated by low excitation power density, which makes it suitable for clinical applications. In the present study, we used biodegradable poly(lactic-co-glycolic acid) (PLGA)-NPs as a delivery vehicle for TTA-UC based on the heavy metal porphyrin Platinum(II) octaethylporphyrin (PtOEP) and the polycyclic aromatic hydrocarbon 9,10-diphenylanthracene (DPA) as a photosensitizer/emitter pair. TTA-UC-PLGA-NPs were successfully synthesized according to an oil-in-water emulsion and solvent evaporation method. After physicochemical characterization, UC-efficacy of TTA-UC-PLGA-NPs was assessed in vitro and ex vivo. TTA-UC could be detected in the tumour area 96 h after in vivo administration of TTA-UC-PLGA-NPs, confirming the integrity and suitability of PLGA-NPs as a TTA-UC in vivo delivery system. Thus, this study provides proof-of-concept that the advantageous properties of PLGA can be combined with the unique optical properties of TTA-UC for the development of advanced nanocarriers for simultaneous in vivo molecular imaging and drug delivery.

Keywords: photon upconversion; triplet-triplet annihilation; in vivo imaging; PLGA; nanoparticles



Citation: Vepris, O.; Eich, C.; Feng, Y.; Fuentes, G.; Zhang, H.; Kaijzel, E.L.; Cruz, L.J. Optically Coupled PtOEP and DPA Molecules Encapsulated into PLGA-Nanoparticles for Cancer Bioimaging. *Biomedicines* **2022**, *10*, 1070. <https://doi.org/10.3390/biomedicines10051070>

Academic Editor: Simon J Allison

Received: 15 March 2022

Accepted: 24 April 2022

Published: 5 May 2022

Publisher's Note: MDPI stays neutral with regard to jurisdictional claims in published maps and institutional affiliations.



Copyright: © 2022 by the authors. Licensee MDPI, Basel, Switzerland. This article is an open access article distributed under the terms and conditions of the Creative Commons Attribution (CC BY) license (<https://creativecommons.org/licenses/by/4.0/>).

1. Introduction

Since the introduction of imaging techniques for the diagnosis and treatment of different pathologies, great progress has been achieved in the field of medical imaging, and the variety of imaging agents has become more sophisticated in terms of efficacy, safety and target specificity [1].

Fluorescence imaging represents a non-invasive imaging technique that can be used to visualize molecular processes and structures in a living organism. Due to advances in biology, organic chemistry and materials science, several types of imaging probes for fluorescent imaging can be distinguished, including small organic dyes, fluorescent proteins and nanoparticles (NPs). NPs are widely used for fluorescent imaging purposes, because of the feasibility of incorporating both hydrophilic and hydrophobic substances, stability, rich contrast and versatility due to surface modification chemistry. For fluorescent materials, there are two kinds of photoluminescence mechanisms, i.e., photon down- and up-conversion (UC) [2]. The conventional down-conversion process normally absorbs one high energy photon and emits a low energy photon, e.g., a Stokes-shift emission. However, down-conversion fluorescence imaging with short-wavelength excitation suffers from

autofluorescence and low signal-to-noise ratio and can cause photo damage to living organisms [3–5]. In the last decade, photon UC has become state of the art in the field of in vitro and in vivo biomedical imaging. Since photon UC is a process that converts low-energy NIR light into high-energy light in the near-infrared (NIR) or visible range [6,7], this process overcomes some of the disadvantages faced by conventional down-conversion probes, with the advantages of (i) large hypsochromic shift, (ii) sharp emission peak, (iii) long luminescence shelf-life, (iv) high photostability, (v) absence of photo damage to living organisms and (vi) high penetration power in biological tissues [8–10]. Photon UC is a combination of photophysical processes, and it can be achieved via different energy transfer mechanisms using different materials, such as rare-earth metals, metalloporphyrins and organic polyaromatic hydrocarbons [6,7].

Triplet-triplet annihilation (TTA) is a special form of UC, resulting in superior optical properties, such as intense absorption of excitation light and high UC quantum yield, while using low excitation power density [7,11,12]; the latter makes TTA-UC particularly interesting for biomedical applications. In TTA-UC, the energy transfer between a sensitizer and an emitter molecule takes place through a series of subsequent nonradiative mechanisms, such as intersystem crossing (ISC) and triplet-triplet energy transfer (TTET, Figure 1) [7,11,12].

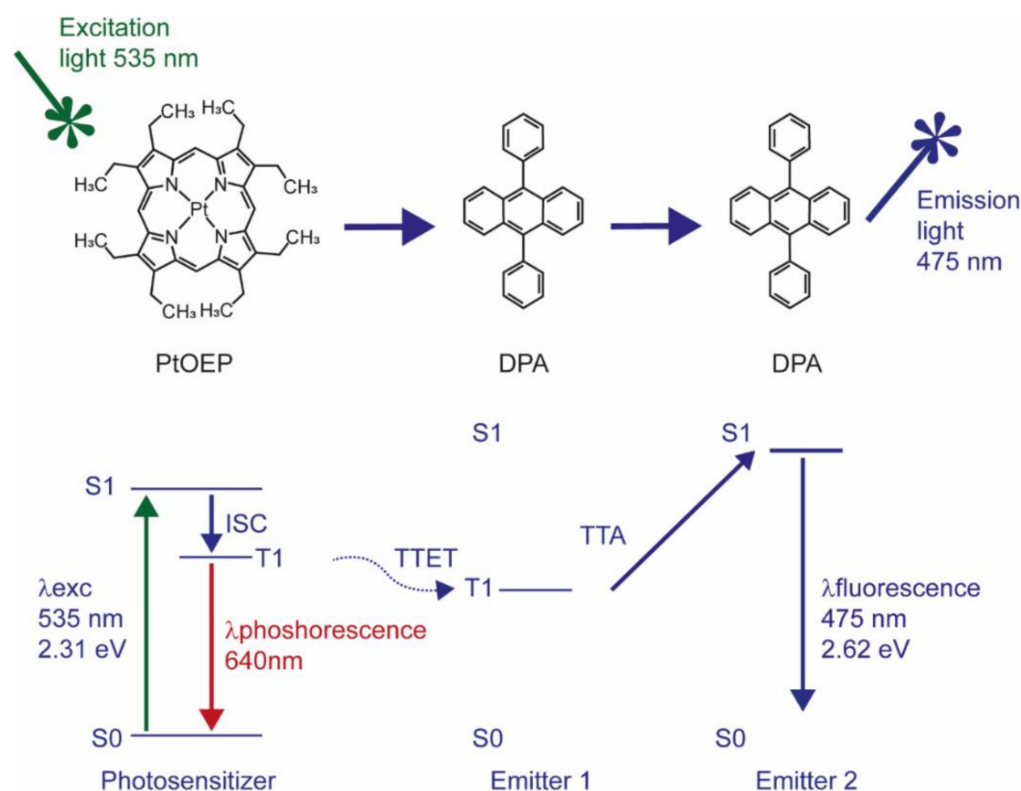


Figure 1. Jablonski diagram describing the energy levels of the electrons involved in energy transfer between PtOEP and DPA molecules. The energy values are calculated based on theoretical data.

When electromagnetic radiation “hits” a sensitizer molecule, its electrons will be promoted from the ground to a singlet excited state and then transferred to a triplet excited state nonradiatively. The released energy that accompanies the transition of the triplet excited electron to the ground singlet state will be transferred to an emitter/acceptor molecule to pump the latter to an excited triplet state. If two of these triplet excited state molecules are close enough, the interaction between the two will cause the transition of one of them to the ground singlet state and the other to a singlet excited state, i.e., the collision results in an annihilation of the triplet excited state of one acceptor molecule and promotion of another one to the singlet excited state (Figure 1).

The UC process is a highly improbable event, according to the quantum mechanical principle, since it consists of a series of spin-forbidden transitions [13]. This means that the UC process should be boosted under favourable conditions that promote those transitions. For instance, to promote ISC, which is the transition of a molecule from a singlet electronic excited state to a triplet electron state, it is advantageous to choose molecules with strong spin-orbit coupling and an expanded π conjugated system. Metalloporphyrins, such as the green absorbing platinum octaethylporphyrin (PtOEP), possess both requirements due to the presence of a transition metal that promotes a spin-forbidden transition and a cyclic π conjugated system that enhances ISC yield [14–16]. More recently, lanthanide complexes of porphyrinoids inside of nanomicelles and mesoporous silica NPs were employed for in vivo imaging in HeLa cells, demonstrating the potential of porphyrinoids as sensitizers in TTA-UC [17].

In the present study, we describe an approach whereby TTA-UC is combined with biocompatible poly(lactic-co-glycolic acid) (PLGA) to create a UC-PLGA-NP system as a potential tool for cancer visualization. NPs, such as those made of biodegradable and FDA-approved PLGA, protect their payload from premature degradation [18–24], are well described and chemically adaptable and can guide their payload inside target cells in vitro and in vivo [23–26].

To generate TTA-UC, we selected PtOEP as the photosensitizer and 9,10-diphenylanthracene (DPA) as the annihilator; a combination that has been reported to result in highly efficient UC yield [27,28]. PtOEP and DPA were successfully encapsulated into the hydrophobic core of PLGA-NPs. Phosphorescence and UC fluorescence signals resulting from TTA-UC-PLGA-NPs could be detected in vitro, in vivo and ex vivo up to 96 h after injection. We conclude that PLGA provides a suitable environment for TTA-UC, which could be utilized for simultaneous optical imaging and drug delivery in vivo.

2. Materials and Methods

2.1. Materials

PtOEP, DPA, DCM and DMF were purchased from Sigma-Aldrich[®], Zwijndrecht, The Netherlands. PLGA 50:50 (PLA/PGA) and water-soluble surfactant, polyvinyl alcohol (PVA), were purchased from Evonik industries AG, Essen, Germany. MTS (3-(4,5-dimethylthiazol-2-yl)-5-(3-carboxymethoxyphenyl)-2-(4-sulfophenyl)-2H-tetrazolium, inner salt) reagent was purchased from Promega, Leiden, The Netherlands. Histomount[™] was purchased from Agar Scientific, Stansted, UK. All aqueous solutions were prepared with Milli-Q water.

2.2. Synthesis of TTA-UC PLGA-NPs Loaded with Metalloporphyrins and Polycyclic Aromatic Hydrocarbons

The TTA-UC-PLGA-NPs were synthesized according to an oil-in-water emulsion and a solvent evaporation method. Briefly, 100 mg of PLGA and 1 mg of each chromophore were dissolved in 3 mL of DCM. The mixture of chromophores and PLGA polymer was emulsified under sonication (ultrasound tip Branson, Sonifier 250), with 25 mL of water containing 500 mg of PVA for 120 s. The newly formed emulsion was left overnight in stirring at 4 °C in order to remove the organic solvent. The PLGA-NPs were collected by centrifugation at 14,800 rpm for 20 min, washed three times and freeze-dried. The NPs were stored at 4 °C and rehydrated prior to use.

2.3. Evaluation of Physicochemical Properties of the TTA-UC-PLGA-NPs

Z-average size, PDI and zeta potential of TTA-UC-PLGA-NPs were measured using a Malvern ZetaSizer 2000, software version number: ZetaSizer 7.03 (Malvern Panalytical Ltd., Malvern, UK). Fixed scattering angle of 90° at 633 nm was set up for the analysis. The measurements were performed after reconstitution of freeze-dried NPs in Milli-Q water.

2.4. Quantification PtOEP and DPA Encapsulation Efficiency

The encapsulation efficiency of chromophores was determined by UV/VIS spectrophotometry using an Ultrospec 2100 pro by Amersham Bioscience. Biodegradable PLGA-NPs were hydrolysed overnight with 0,8 M NaOH at 37 °C. Concentration of dyes was calculated using a calibration curve built with known amounts of PtOEP and DPA.

2.5. Cell Culture

The human ovarian carcinoma cell line OVCAR-3 and the breast cancer cell line MCF-7 (both cell lines, from ATCC, Manassas, VA, USA) were cultured in RPMI (Roswell Park Memorial Institute 1640 Medium) medium supplemented with 10% foetal calf serum. The cells were left to attach to the bottom of the plate for 4 h before treatment with NPs. After 4 h, the NPs were added to the cells at various concentrations of 25, 50, 100, and 200 µg/mL. DMSO at 25% was used as a positive control. The cells treated with NPs were incubated at 37 °C under 5% CO₂ for 72 h. After 72 h, the medium was changed, and 20 µL of MTS reagent was added to each well. The ELISA reader (Molecular Devices VERSAmax Tunable Microplate Reader, Software: SoftMax Pro v5.4.1) was used to measure the absorbance value of MTS product at 490 nm when the colour of the medium changed from yellow to light brown. The following formula was applied to calculate the viability of cell growth: cell viability (%) = (mean of absorbance value of treated sample/mean of absorbance of negative (live) control) × 100.

2.6. In Vitro Uptake of TTA-UC-PLGA-NPs by OVCAR-3 Cells

Fluorescence imaging of fixed OVCAR-3 cells incubated with TTA-UC-PLGA-NPs was performed with a Leica DMRA microscope using a PL APO 63x/1.32-0.6 oil objective. DAPI and Cy5 filters were used for nucleus and membrane detection, respectively, using the following protocol: Adherent cells were detached with 0.2% trypsin in PBS (Gibco by Life Technologies, Bleiswijk, The Netherlands) and seeded in 8-well chamber slides (BD Biosciences, Franklin Lakes, NJ, USA) at a concentration of 2×10^4 cells/well. After 4 h, the TTA-UC-PLGA-NPs were added at a concentration of 200 µg/mL for 2 h at 37 °C under 5% of CO₂. At the end of the incubation time, the cells were washed with PBS, fixed in 4% of paraformaldehyde (PFA) and stained with DiD labelling solution according to manufacturer's protocol (Invitrogen, The Netherlands). The staining was completed adding Vectashield mounting medium containing DAPI.

2.7. Measurement of UC Process

Confocal microscopy imaging of TTA-UC-PLGA-NPs was performed by a Leica SP8 X WLL (White Light Laser) laser scanning microscope. To this end, TTA-UC-PLGA-NPs were dissolved at 5 µg/µL in distilled water and dropped onto a glass slide and imaged. Emissions were collected between 650–670 nm and 430–475 nm; the excitation was provided at 535 nm.

2.8. Stability Measurement of TTA-UC-PLGA-NPs in Solution

In order to evaluate the stability of the TTA-UC system inside the PLGA core, the TTA-UC-PLGA-NPs were dissolved in PBS and left for 0, 24 and 72 h shaking (300 rpm) at 37 °C. At each time point, phosphorescence and UC-luminescence were measured using a spectrofluorometer (Fluorolog). The suspension of TTA-UC-PLGA-NPs was excited at 535 nm, and the emission signals were captured at 433 and 641 nm.

2.9. Animals

All the animal studies were in conformity with the animal management protocols and were approved by the Leiden University Animal Experimental Committee; studies were performed in accordance with the national legislation of the Netherlands and in compliance with the 'Code of Practice Use of Laboratory Animals in Cancer Research' (Inspectie W&V, July 1999). Female FVB mice were purchased from Charles River Laboratories

(L'Arbresle Cedex, France). Animals were housed at 22 °C and 50% humidity, with free access to food and water, and maintained under standard 12 h light/12 h dark cycles. All animal experiments were assessed according to the ethics of animal research and approved by the Animal Welfare Committee of Leiden University Medical Center, the Netherlands. All mice received humane care and were kept in compliance with the Code of Practice Use of Laboratory Animals in Cancer Research (Inspectie W&V, July 1999). All analytical procedures were performed under isoflurane gas anaesthesia (3% induction, 1.5–2% maintenance) in 70% pressurized air and 30% O₂, unless stated differently.

2.10. In Vivo Monitoring of TTA-UC-PLGA-NPs

In vivo imaging was performed using the IVIS spectrum Preclinical Imaging System (Caliper LS, Hopkinton, MA, USA). The images were analysed with Living Image 4.3.0 software. First, the tumour was induced by injecting 1×10^6 MCF cells in 100 μ L PBS subcutaneously into the back of the mice. When the tumours reached the volume of approximately 125 mm³, 0.5 mg TTA-UC-PLGA-NPs in 100 μ L PBS were injected into the tail vein of each mouse. At 3, 24, 72 and 96 h post injection, optical imaging of treated mice was performed. Biodistribution kinetics at each time point were measured by quantifying the fluorescence intensity in pre-set regions of interest (ROIs) at the tumour site, expressed as the average radiant efficiency in (p/sec/cm²/sr)/(μ W/cm²).

2.11. Measurement of TTA-UC Ex Vivo

After 96 h, the mice were sacrificed and subcutaneous tumours were surgically removed. Freshly isolated tumours were placed in tissue moulds and covered with Tissue-Tek[®] O.C.T.[™] (Sakura). For snap freezing, the tumours were left on dry ice for some minutes and then stored at –80 °C. Cryosectioning of tumours was performed using CryoStar[™] NX70 at a working temperature between –25 and –30 °C; the thickness of the sections was fixed between 5 and 14 μ m. Before microscopic analysis of the tumours, the sections were washed in Milli-Q water, dried under the hood and mounted in medium containing Mowiol (Sigma) and 2.5% DABCO (Sigma).

2.12. Statistical Data Analysis

Graph Pad Prism software version 7 was used to perform statistical analysis. The Mann–Whitney test was applied in all experiments.

3. Results and Discussion

3.1. Preparation, Physicochemical Characterization and Cytotoxicity of TTA-UC-PLGA-NPs

In the present study, TTA-UC-PLGA-NPs were successfully synthesized by applying an oil-in-water emulsion and solvent evaporation method, as previously described [23,24,26,29]. Briefly, 100 mg of PLGA and 1 mg of each chromophore were dissolved in 3 mL of dichloromethane (DCM). The mixture of chromophores and PLGA polymer was emulsified under sonication in the presence of PVA. After removal of the organic solvent, the TTA-UC-PLGA-NPs were collected by centrifugation, washed and freeze-dried. The oil-in-water emulsion and solvent evaporation method led to an encapsulation efficiency (EE) of PtOEP and DPA molecules of 24% and 40%, respectively, as determined by nanodrop measurement of dissolved NPs (Table 1).

Table 1. Physicochemical properties of NPs. Data are presented as average \pm SD (N = 3).

| NPs | Size (nm) | ζ (mV) | PDI | Loading (μ g/mg) | Encapsulation Efficiency (%) |
|-------------|--------------|--------------|-----|-------------------------|------------------------------|
| Blank PLGA | 180 \pm 80 | –24 \pm 6 | 0.2 | - | - |
| TTA-UC PLGA | 200 \pm 50 | –31 \pm 5 | 0.4 | PtOEP: 244.0 DPA: 396.0 | PtOEP: 24.4 DPA: 39.6 |

Due to the high sensitivity of the porphyrin triplet states to oxygen quenching, the actual lifetime of the triplet state depends on the solvent, its purity and its oxygen content [30]. To protect the optical properties of chromophores, PtOEP and DPA were dissolved in DCM. To ensure that encapsulation into PLGA-NPs did not affect the optical properties of PtOEP and DPA, TTA-UC-PLGA-NPs were dissolved in dimethylformamide (DMF), analysed by absorption curve analysis and compared to pure compounds (Figure 2).

The absorption spectrum of PtOEP depicts the characteristic shape of porphyrin absorption: a strong absorption peak at 380 nm (Soret band) was accompanied by a weaker absorption peak located at 501 and 533 nm (Q-band) (Figure 2A) [31]. DPA, the emitter for the TTA-UC system, showed several absorption peaks between 350 nm and 400 nm (Figure 2B).

When the TTA-UC-PLGA-NPs were dissolved in DMF, the absorption spectrum showed the combined characteristic optical profiles of PtOEP and DPA (Figure 2C). In conclusion, absorption spectrum analysis of TTA-UC-PLGA-NPs confirmed the successful encapsulation of both chromophores into the PLGA polymer, while the optical properties of PtOEP and DPA were maintained.

The size of the NPs was determined by dynamic light scattering (DLS) analysis as ~200 nm in diameter (Table 1, Figure 3A), and the polydispersity index (PDI) value of 0.4 obtained from the DLS measurement indicated a homogeneous size distribution (Table 1). Compared to blank control PLGA-NPs, the diameter of the NPs slightly increased upon encapsulation of PtOEP and DPA.

NPs smaller than 10 nm are known to be eliminated by renal excretion [32], while NPs with sizes ranging from 50 to 300 nm show extended circulation times in the blood stream compared to NPs of larger size [33]. Hence, TTA-UC-PLGA-NPs of 200 nm have the ideal size for prolonged systemic circulation times; an important prerequisite to reach the tumour site. In addition, ZetaSizer measurement showed that the surface charge of the NPs was on average -30 mV (Table 1, Figure 3B).

The surface charge is a crucial factor to determine the stability of the NPs in solution, but also affects cellular uptake, biodistribution and cytotoxicity. A high surface charge guarantees an electrostatic stabilization of the NPs due to a strong surface repulsion between NPs of the same charge. According to the measured value, it is possible to assume that the NPs are stable in suspension for a prolonged period of time [34].

Next, we investigated the optical properties of the TTA-UC system after encapsulation into PLGA-NPs. To this purpose, TTA-UC-PLGA-NPs were dissolved in water and excited at 535 nm (Figure 3C). The detected TTA-UC signal at 433 nm was similar to that previously reported for PtOEP/DPA systems [35], thus confirming the integrity of the TTA-UC system after encapsulation into PLGA.

The charge of UC-NPs has been shown to affect the intracellular localization and cellular cytotoxicity [31]. Positively charged UC-NPs localize to mitochondria, while negatively charged UC-NPs preferentially localize to lysosomes and the cytoplasm, which is associated with lower cellular cytotoxicity [36]. To assess the potential toxicity of our NPs, TTA-UC-PLGA-NPs were incubated at different concentrations (25–200 $\mu\text{g}/\text{mL}$) for 72 h with OVCAR-3 ovarian cancer cells, and the cellular toxicity was determined by MTS assay (Figure 4). TTA-UC-PLGA-NPs were compared to empty control PLGA-NPs. No toxicity of TTA-UC-PLGA-NPs or empty PLGA-NPs on OVCAR-3 cells was observed after 72 h (Figure 4).

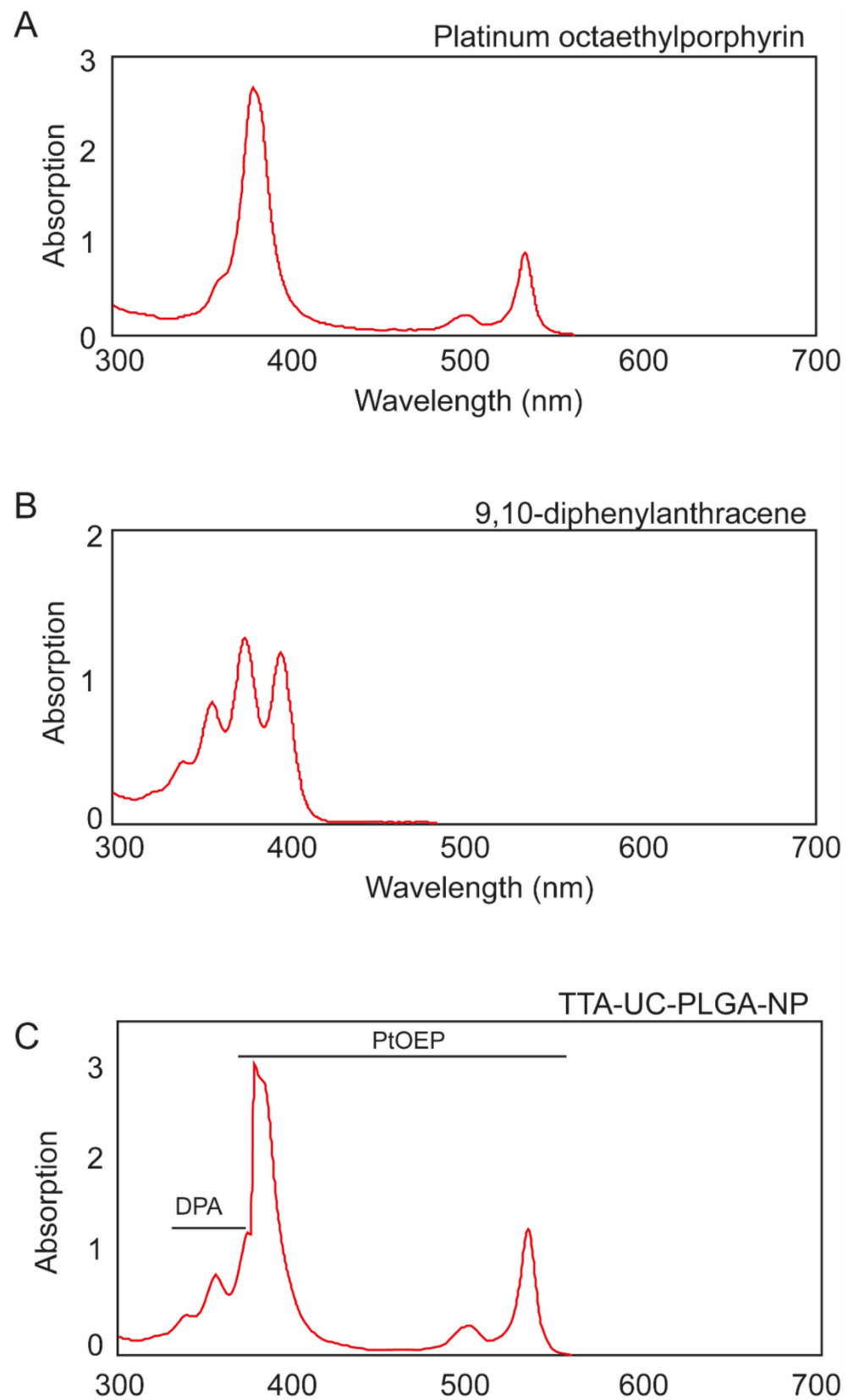


Figure 2. Individual absorption spectra of (A) platinum octaethylporphyrin (PtOEP) and (B) 9,8-diphenylanthracene (DPA), each dissolved in dimethylformamide (DMF). (C) TTA-UC-PLGA-NPs were hydrolysed overnight in 0.8 M NaOH at 37 °C, and the absorption spectrum of co-encapsulated PtOEP and DPA was measured.

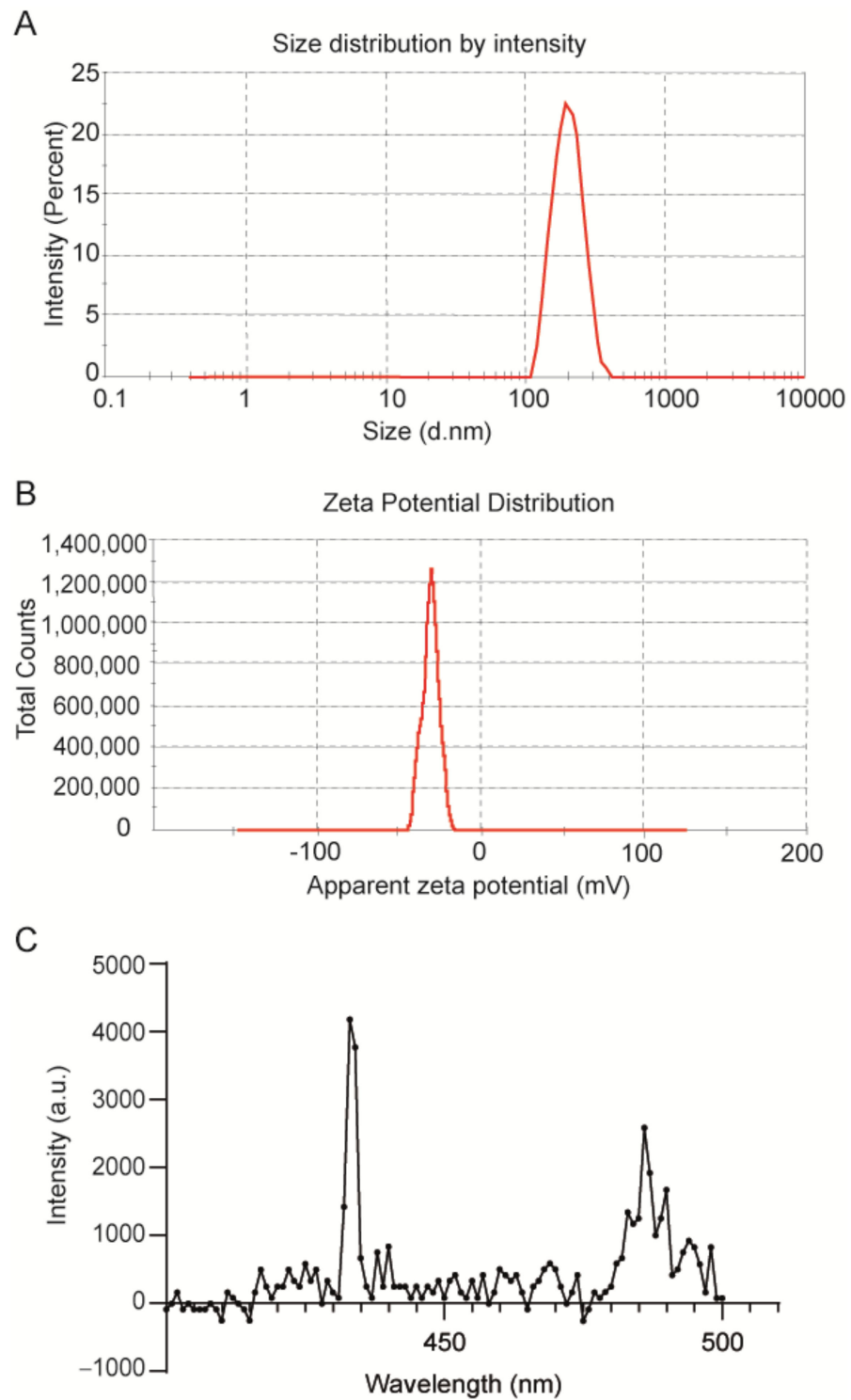


Figure 3. Physicochemical characterization of TTA-UC-PLGA-NPs. Representative (A) dynamic light scattering and (B) zeta-potential measurement of TTA-UC-PLGA-NPs reconstituted in water after freeze-drying. The average size of the nanoparticles was 198 nm in diameter, and the average zeta potential value was -31 mV. (C) TTA-UC-PLGA-NPs were dissolved in water and directly analysed. The NPs in solution were excited at 535 nm, and the emission was collected using a photofluorometer.

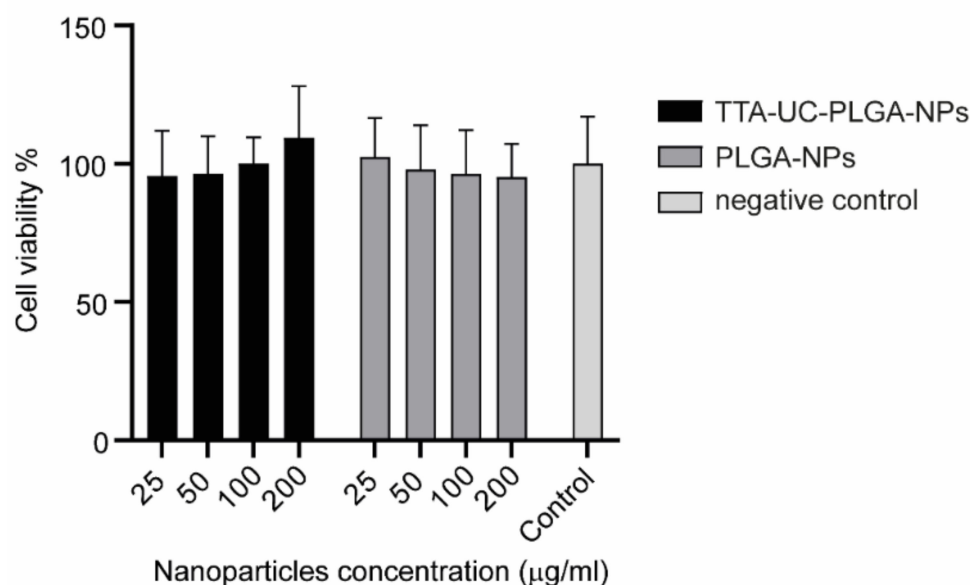


Figure 4. Assessment of cellular cytotoxicity of TTA-UC-PLGA-NPs. OVCAR-3 cells were incubated with 25, 50, 100 and 200 µg/mL TTA-UC-PLGA-NPs or control PLGA-NPs for 72 h. Untreated cells were used as negative control. The cell viability was assessed after 72 h by MTS assay.

3.2. Cellular Uptake of TTA-UC-PLGA-NPs Characterized by Fluorescence Microscopy

To assess the cellular uptake of TTA-UC-PLGA-NPs, OVCAR-3 cells were incubated for 2 h with 200 µg/mL TTA-UC-PLGA-NPs and analysed by fluorescent microscopy. In order to confirm the intracellular localization of the NPs, the cells were counterstained with DAPI ($\lambda_{\text{excitation}} = 340\text{--}380$ nm, $\lambda_{\text{emission}} = 425$ nm) and DiD ($\lambda_{\text{excitation}} = 676\text{--}688$ nm, $\lambda_{\text{emission}} = 700\text{--}742$ nm) for nucleus and membrane detection, respectively.

To detect the TTA-UC-PLGA-NPs, the samples were excited at 542–582 nm, and the phosphorescence signal was collected at 604–644 nm (Figure 5). TTA-UC-PLGA-NPs were successfully taken up by OVCAR-3 cells. The overlay of the membrane staining with the phosphorescence signal of the TTA-UC-PLGA-NPs confirmed the intracellular localization of the NPs (Figure 5).

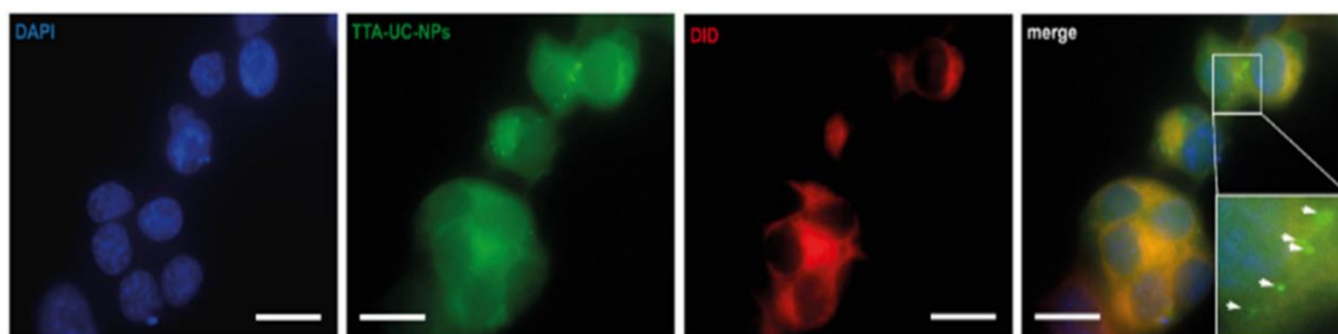


Figure 5. Cellular uptake of TTA-UC-PLGA-NPs. OVCAR-3 cells were incubated with 200 µg/mL TTA-UC-PLGA-NPs for 2 h at 37 °C and analysed by fluorescence microscopy. The cells were fixed, and the nucleus was stained with DAPI (blue) and the cell membrane was stained with DiD (red). The phosphorescence signal (green) of the TTA-UC-PLGA-NPs was collected. The following filter cubes were used to discriminate DAPI, DiD and TTA-UC-PLGA-NP-signals: DAPI, $\lambda_{\text{exc}} = 340\text{--}380$ nm and $\lambda_{\text{emi}} = 425$ nm; DiD, $\lambda_{\text{exc}} = 676\text{--}688$ nm, $\lambda_{\text{emi}} = 700\text{--}742$ nm; TTA-UC-PLGA-NPs, $\lambda_{\text{exc}} = 542\text{--}582$ nm, $\lambda_{\text{emi}} = 604\text{--}644$ nm. Scale bar = 20 µm.

3.3. Characterization of TTA-UC-PLGA-NPs UC Properties

The ability of TTA-UC-PLGA-NPs to generate the UC process was assessed by confocal microscopy (Figure 6). The NPs were excited at a wavelength of 535 nm, and the emission signals were collected between 430–475 nm and 650–670 nm. In our study, the emission shift towards shorter wavelengths (hypsochromic shift) went from green (535 nm) to blue (430–475 nm) (Figure 6). This means that the energy associated with the emission wavelength was higher than the energy associated with the excitation wavelength, as a consequence of the anti-Stokes shift in the TTA-UC process [37]. On the contrary, the change in emission spectrum towards longer wavelengths (bathochromic shift), in our case 650–670 nm, is a characteristic of all conventional luminescence processes (Figure 6). Using confocal microscopy, we could image the single TTA-UC-PLGA-NPs that created dual emission wavelengths: the red emission from the phosphorescence of PtOEP and the blue emission as a result of the TTA-UC process. Thus, we confirmed the preparation of functional TTA-UC-PLGA-NPs.

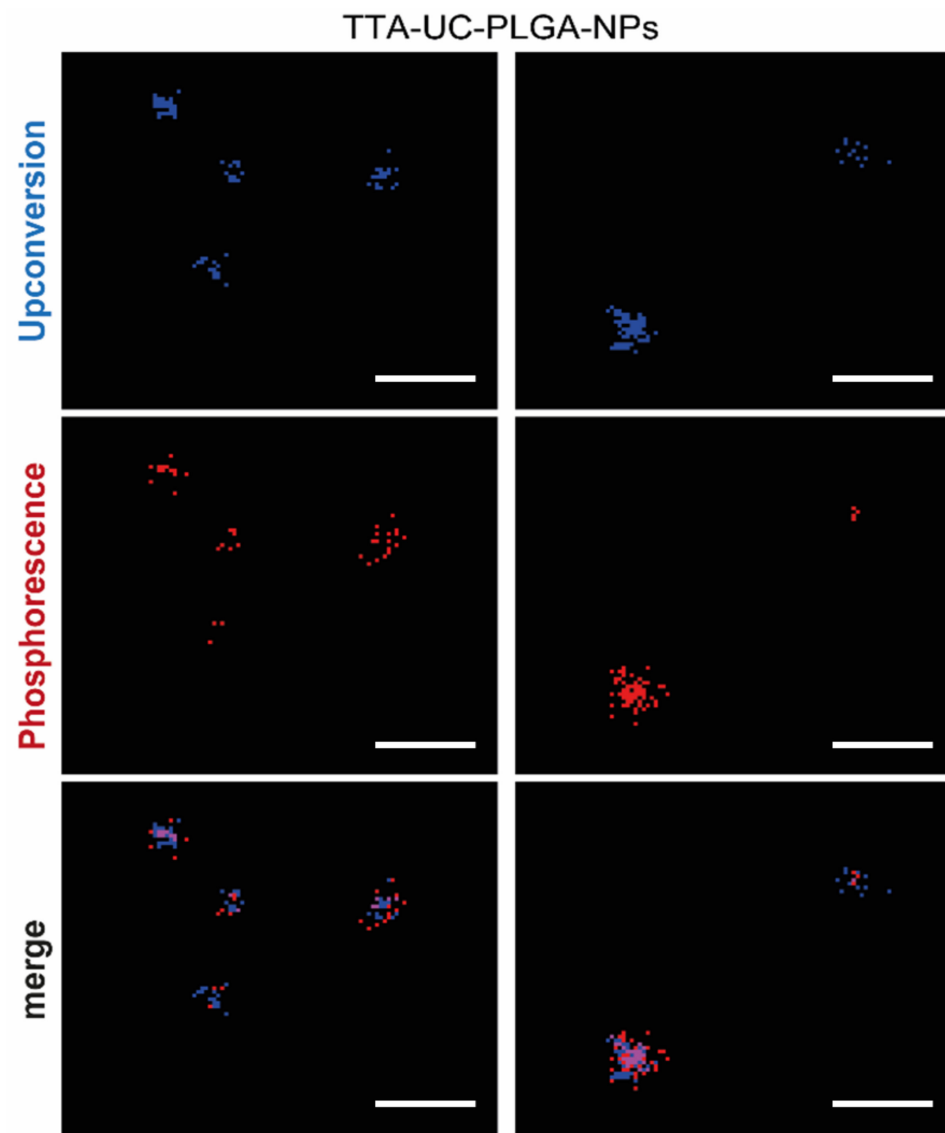


Figure 6. TTA-UC imaged by confocal microscopy. UC-TTA-PLGA-NPs were dissolved in water and imaged on a glass cover slip. The NPs were excited at 535 nm, and the following emission wavelengths were collected: 430–475 nm (blue) = upconversion, 650–670 nm (red) = phosphorescence. Scale white bar = 10 μ m.

The dual colour feature of TTA-UC-PLGA-NPs was useful to improve signal-to-noise ratio and to estimate the ratio of the UC/phosphorescence signal. The overall efficiency of the TTA-UC process depends on each elementary step (ISC, TTET, TTA), on the concentration of emitter molecules and on the presence of other competing molecules, such as elementary oxygen [11,30]. Additional challenges are encountered with when TTA-UC is integrated in an NP system. Aggregation of photosensitizers and emitters can have detrimental effects on the optical properties of TTA-UC-NPs, and as a consequence, the loss of mobility of photosensitizers/emitters can limit the UC process [11,38]. Thus, creating a highly efficient UC-NP system without any secondary decay remains an enormous challenge for practical application [39].

3.4. Assessment of TTA-UC-PLGA-NP Optical Properties in Solution

Next, we investigated the optical properties of TTA-UC-PLGA-NPs over time. To this purpose, TTA-UC-PLGA-NPs were dissolved in PBS and incubated at 37 °C in shaking mode. At time point 0, 24 and 72 h, the dispersion of TTA-UC-PLGA-NPs was excited at 535 nm, and the TTA-UC and phosphorescence processes were measured at 433 and at 642 nm, respectively (Figure 7).

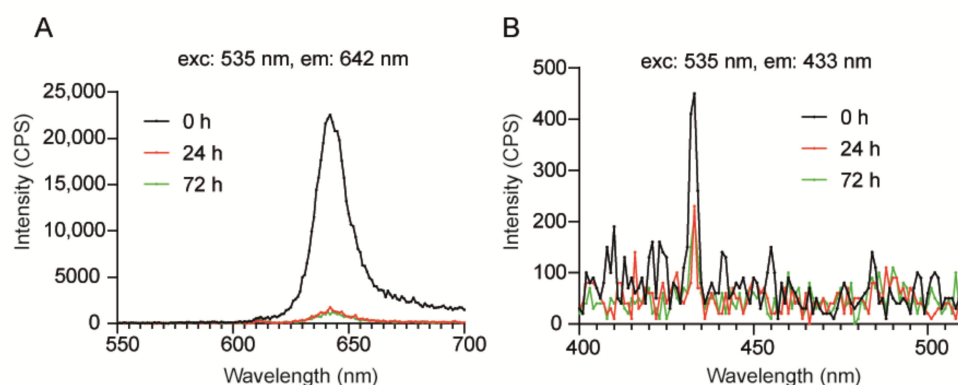


Figure 7. Assessment of optical properties of TTA-UC-PLGA-NPs in solution. TTA-UC-PLGA-NPs were dissolved in water and incubated at 37 °C for 72 h. At time point 0, 24 and 72 h, samples were analysed. The NPs in solution were excited at 535 nm, and the emission was collected using a photofluorometer. **(A)** Phosphorescence and **(B)** TTA-UC emission graphs of TTA-UC-PLGA-NPs at various time points.

The strongest phosphorescence and TTA-UC signals were detected at time point 0 (0 h post dissolution) (Figure 7A). After 24 h, the phosphorescence and TTA-UC signals decreased but could still be detected after 72 h incubation at 37 °C. Thus, the data demonstrates that TTA-UC-PLGA-NPs are suitable for imaging processes lasting for at least 72 h. As PLGA-NPs have been reported to be stable under physiological conditions for extended periods of time [40], the initial decrease in TTA-UC/phosphorescence intensity within the first 24 h observed here is likely the result of diffusion of the chromophores out of the PLGA-core.

3.5. In Vivo Monitoring of TTA-UC-PLGA-NPs

Real-time imaging of FVB mice was carried out with the goal to trace TTA-UC-PLGA-NPs in cancer cells in vivo. To this end, the IVIS imaging system was employed, which allowed measurement of the bathochromic emission captured at 640 nm (but not the UC process).

FVB mice were inoculated in the back with 1×10^6 human breast adenocarcinoma cells (MCF). When the tumours reached a volume of approximately 125 mm³, TTA-UC-PLGA-NPs were injected intravenously in the tail vein. At different time points post injection (3, 24, 48, 72 and 96 h), the mice were imaged using a whole-body fluorescent imaging

system. In vivo imaging data showed that already at 3 h post injection, TTA-UC-PLGA-NPs accumulated in the tumour area (Figure 8A).

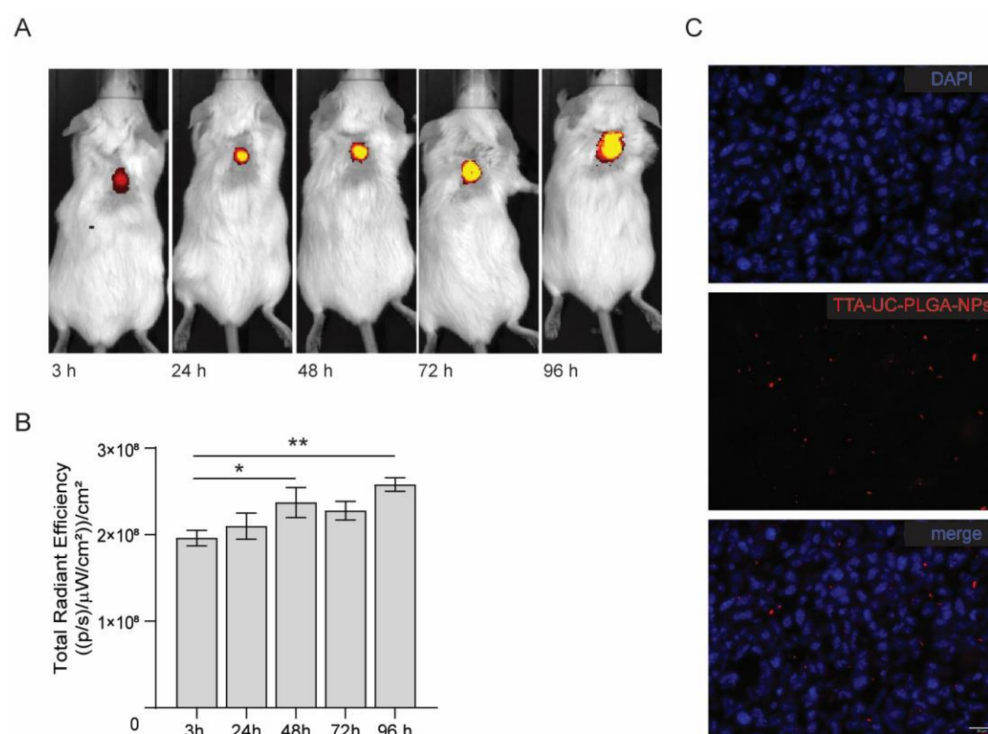


Figure 8. In vivo imaging of TTA-UC-PLGA-NPs. (A) FVB mice were inoculated in the back with 1×10^6 MCF-7 cells. When the tumours reached a size of 125 mm^3 , mice were injected intravenously in the tail vein with 0.5 mg of TTA-UC-PLGA-NPs and imaged 3, 24, 48, 72 and 98 h post injection using the IVIS imaging system. (A) TTA-UC-PLGA-NPs were excited at a wavelength of 535 nm, and the emission (phosphorescence) was collected at 640 nm. (B) The total radiance efficiencies were calculated in the tumour areas, and the values were compared. Statistical analysis was performed using the Mann–Whitney test, * $p = 0.026$, ** $p = 0.0022$ (6 mice per group were used). (C) MCF-tumours were excised 96 h post injection of TTA-UC-PLGA-NPs and tumour cryosections were imaged by fluorescent microscopy. The following filter cubes were used to discriminate DAPI (blue) and TTA-UC-PLGA-NPs (red) signals: DAPI, $\lambda_{\text{exc}} = 340\text{--}380 \text{ nm}$ and $\lambda_{\text{emi}} = 425 \text{ nm}$; TTA-UC-PLGA-NPs, $\lambda_{\text{exc}} = 542\text{--}582 \text{ nm}$, $\lambda_{\text{emi}} 604\text{--}644 \text{ nm}$. Scale bar = 20 μm .

The mice were monitored up to 96 h post injection. As the IVIS imaging system is not equipped to detect the emission between 430–450 nm, we instead measured the phosphorescence signal, which could be detected during all imaged time points (Figure 8A,B). Quantification of the signal showed a significant increase in phosphorescence signal in the tumour area in the first 48 h ($p = 0.026$) and after 96 h ($p = 0.0022$), indicating that more TTA-UC-PLGA-NPs accumulated at the tumour site over time.

The presence of TTA-UC-PLGA-NPs in the tumour at endpoint was confirmed by fluorescent imaging of tumour cryosections (Figure 8C). Moreover, the data showed that once accumulated in the tumour, the NPs remained at the tumour site. Since the NPs did not present any specific targeting moiety for breast adenocarcinoma cancer cells, TTA-UC-PLGA-NPs most likely accumulated at the tumour site via the EPR effect. Tumour blood vessels are naturally leaky, with large openings up to 1.5 mm, thereby promoting the passive accumulation of NPs in tumours [41,42].

3.6. Measurement of TTA-UC Process Ex Vivo

At 96 h post TTA-UC-PLGA-NP injection, breast adenocarcinoma tumours were excised, and the presence of TTA-UC phenomenon was analysed ex vivo. To this end,

isolated tumours were further processed for cryosectioning and imaged using a confocal microscope. The sections were excited at 514 nm, and emissions were collected between 430–475 nm (to observe TTA-UC) and 650–670 nm (to observe phosphorescence) (Figure 9).

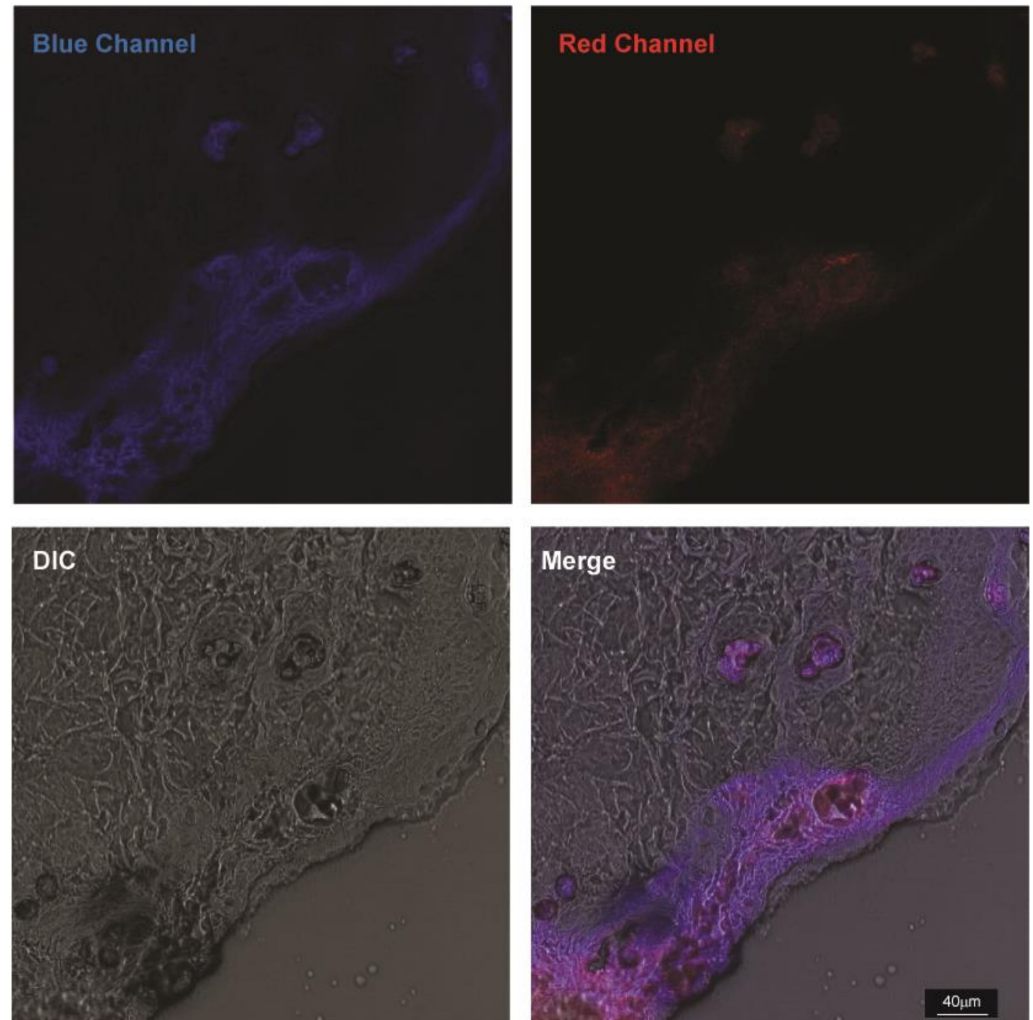


Figure 9. Ex vivo imaging of TTA-UC-PLGA-NPs. MCF-tumours were excised 96 h post injection of TTA-UC-PLGA-NPs and tumour cryosections were imaged by confocal microscopy. All cryosections were excited at 514 nm, and the upconversion signal (blue channel) was collected between 430–475 nm and the phosphorescence signal (red channel) between 650–670 nm. Scale bar = 40 μm .

Strikingly, TTA-UC and phosphorescence signals could be detected in the tumour margins and vessel-like structures 96 h post injection of TTA-UC-PLGA-NPs. The staining pattern suggests that TTA-UC-PLGA-NPs diffused into the tumour via the margins and entered into deeper tumour areas via leakages in the tumour vasculature. The data further confirmed that, despite initial diffusion of chromophores out of the PLGA copolymers (Figure 7), the integrity of TTA-UC-PLGA-NPs was maintained for at least 96 h in vivo.

4. Conclusions

In the present study, we developed a TTA-UC-PLGA-NP system by incorporating the polycyclic aromatic hydrocarbon DPA and the metalporphyrin PtOEP into a core of hydrophobic PLGA-copolymers. In vitro and ex vivo studies confirmed the presence of TTA-UC phenomenon resulting from TTA-UC-PLGA-NPs. TTA-UC could be detected 96 h post injection of TTA-UC-PLGA-NPs in the tumour area in vivo, confirming the integrity and suitability of PLGA-NPs as in vivo delivery system for TTA-UC, while maintaining

the optical integrity of the TTA-UC process. This study provides proof-of-concept evidence on the feasibility of combining the advantageous properties of PLGA for drug delivery with state-of-the-art TTA-UC for simultaneous optical in vivo imaging. The presented methodology could form the basis for novel TTA-UC systems encapsulated into PLGA, which can be excited in the NIR-I or NIR-II range for clinical translation.

Author Contributions: O.V., C.E. and L.J.C. conceived the study and were in charge of the study methodology; O.V., C.E., H.Z. and L.J.C. were involved in formal analysis and investigation; O.V., C.E., Y.F. and G.F. were involved in data curation; O.V., C.E., Y.F., G.F. and E.L.K. were in charge of drafting the manuscript; O.V., C.E., G.F., H.Z., E.L.K. and L.J.C. were involved in writing, reviewing and editing of the manuscript; C.E. and L.J.C. provided the study resources and were in charge of supervision, project administration and funding acquisition. All authors have read and agreed to the published version of the manuscript.

Funding: O.V. and L.J.C. were supported by project grants from the European Commission: Marie Skłodowska Curie grant agreement CANCER (777682), PRISAR2 (872860), ACORN (807281), SIMICA (852985), BIOSAFETY (952520), PAVE (861190), CAST (857894), NOVA-MRI (859908), PIANO (956477). C.E. was supported by the H2020-WIDESPREAD-2018-03 SIMICA (852985—) project grant from the European Commission, and the Dutch PPS allowance made available by Health~Holland, Top Sector Life Sciences & Health for the project NANOCAS T 2.

Institutional Review Board Statement: All animal experiments were assessed according to the ethics of animal research and approved by the Animal Welfare Committee of Leiden University Medical Center, the Netherlands. All mice received humane care and were kept in compliance with the Code of Practice Use of Laboratory Animals in Cancer Research (Inspectie W&V, July 1999).

Informed Consent Statement: Not applicable.

Data Availability Statement: Not applicable.

Conflicts of Interest: The authors declare no conflict of interest.

References

1. Kinch, M.S.; Woodard, P.K. Analysis of FDA-approved imaging agents. *Drug Discov. Today* **2017**, *22*, 1077–1083. [[CrossRef](#)] [[PubMed](#)]
2. Pratiwi, F.W.; Kuo, C.W.; Chen, B.-C.; Chen, P. Recent advances in the use of fluorescent nanoparticles for bioimaging. *Nanomedicine* **2019**, *14*, 1759–1769. [[CrossRef](#)]
3. Li, Z.; Sun, Q.; Zhu, Y.; Tan, B.; Xu, Z.P.; Dou, S.X. Ultra-small fluorescent inorganic nanoparticles for bioimaging. *J. Mater. Chem. B* **2014**, *2*, 2793–2818. [[CrossRef](#)] [[PubMed](#)]
4. Rubio-Camacho, M.; Alacid, Y.; Mallavia, R.; Martínez-Tomé, M.J.; Mateo, C.R. Polyfluorene-Based Multicolor Fluorescent Nanoparticles Activated by Temperature for Bioimaging and Drug Delivery. *Nanomaterials* **2019**, *9*, 1485. [[CrossRef](#)] [[PubMed](#)]
5. Thangudu, S.; Kalluru, P.; Vankayala, R. Preparation, Cytotoxicity, and In Vitro Bioimaging of Water Soluble and Highly Fluorescent Palladium Nanoclusters. *Bioengineering* **2020**, *7*, 20. [[CrossRef](#)] [[PubMed](#)]
6. Chen, G.; Qiu, H.; Prasad, P.N.; Chen, X. Upconversion Nanoparticles: Design, Nanochemistry, and Applications in Theranostics. *Chem. Rev.* **2014**, *114*, 5161–5214. [[CrossRef](#)]
7. Zuo, J.; Tu, L.; Li, Q.; Feng, Y.; Que, I.; Zhang, Y.; Liu, X.; Xue, B.; Cruz, L.J.; Chang, Y.; et al. Near Infrared Light Sensitive Ultraviolet–Blue Nanophotoswitch for Imaging-Guided “Off–On” Therapy. *ACS Nano* **2018**, *12*, 3217–3225. [[CrossRef](#)]
8. Nguyen, P.-D.; Son, S.J.; Min, J. Upconversion Nanoparticles in Bioassays, Optical Imaging and Therapy. *J. Nanosci. Nanotechnol.* **2014**, *14*, 157–174. [[CrossRef](#)]
9. Singh, R.; Dumlupinar, G.; Andersson-Engels, S.; Melgar, S. Emerging applications of upconverting nanoparticles in intestinal infection and colorectal cancer. *Int. J. Nanomed.* **2019**, *14*, 1027–1038. [[CrossRef](#)]
10. Rauch, M.P.; Knowles, R.R. Applications and Prospects for Triplet-Triplet Annihilation Photon Upconversion. *CHIMIA Int. J. Chem.* **2018**, *72*, 501–507. [[CrossRef](#)]
11. Huang, L.; Kakadiaris, E.; Vaneckova, T.; Huang, K.; Vaculovicova, M.; Han, G. Designing next generation of photon upconversion: Recent advances in organic triplet-triplet annihilation upconversion nanoparticles. *Biomaterials* **2019**, *201*, 77–86. [[CrossRef](#)] [[PubMed](#)]
12. Zhou, J.; Liu, Q.; Feng, W.; Sun, Y.; Li, F. Upconversion Luminescent Materials: Advances and Applications. *Chem. Rev.* **2015**, *115*, 395–465. [[CrossRef](#)] [[PubMed](#)]
13. Zhu, X.; Su, Q.; Feng, W.; Li, F. Anti-Stokes shift luminescent materials for bio-applications. *Chem. Soc. Rev.* **2017**, *46*, 1025–1039. [[CrossRef](#)] [[PubMed](#)]

14. Borisov, S.M.; Saf, R.; Fischer, R.; Klimant, I. Synthesis and Properties of New Phosphorescent Red Light-Excitable Platinum(II) and Palladium(II) Complexes with Schiff Bases for Oxygen Sensing and Triplet–Triplet Annihilation-Based Upconversion. *Inorg. Chem.* **2013**, *52*, 1206–1216. [[CrossRef](#)] [[PubMed](#)]
15. Han, J.; Duan, P.; Li, X.; Liu, M. Amplification of Circularly Polarized Luminescence through Triplet–Triplet Annihilation-Based Photon Upconversion. *J. Am. Chem. Soc.* **2017**, *139*, 9783–9786. [[CrossRef](#)]
16. Sguerra, F.; Bulach, V.; Hosseini, M.W. Molecular tectonics: Zinc coordination networks based on centric and acentric porphyrins bearing pyridyl units. *Dalton Trans.* **2012**, *41*, 14683–14689. [[CrossRef](#)]
17. Yang, Z.-S.; Ning, Y.; Yin, H.-Y.; Zhang, J.-L. Lutetium(III) porphyrinoids as effective triplet photosensitizers for photon upconversion based on triplet–triplet annihilation (TTA). *Inorg. Chem. Front.* **2018**, *5*, 2291–2299. [[CrossRef](#)]
18. Kim, J.; Hong, J.; Lee, J.; Fakhraei Lahiji, S.; Kim, Y.-H. Recent advances in tumor microenvironment-targeted nanomedicine delivery approaches to overcome limitations of immune checkpoint blockade-based immunotherapy. *J. Control. Release* **2021**, *332*, 109–126. [[CrossRef](#)]
19. Phung, C.D.; Tran, T.H.; Kim, J.O. Engineered nanoparticles to enhance natural killer cell activity towards onco-immunotherapy: A review. *Arch. Pharm. Res.* **2020**, *43*, 32–45. [[CrossRef](#)]
20. Li, W.; Liu, Z.; Fontana, F.; Ding, Y.; Liu, D.; Hirvonen, J.T.; Santos, H.A. Tailoring Porous Silicon for Biomedical Applications: From Drug Delivery to Cancer Immunotherapy. *Adv. Mater.* **2018**, *30*, 1703740. [[CrossRef](#)]
21. Liu, L.; Li, H.; Wang, J.; Zhang, J.; Liang, X.-J.; Guo, W.; Gu, Z. Leveraging macrophages for cancer theranostics. *Adv. Drug Deliv. Rev.* **2022**, *183*, 114136. [[CrossRef](#)] [[PubMed](#)]
22. Rueda, F.; Eich, C.; Cordobilla, B.; Domingo, P.; Acosta, G.; Albericio, F.; Cruz, L.J.; Domingo, J.C. Effect of TLR ligands co-encapsulated with multiepitopic antigen in nanoliposomes targeted to human DCs via Fc receptor for cancer vaccines. *Immunobiology* **2017**, *222*, 989–997. [[CrossRef](#)] [[PubMed](#)]
23. Da Silva, C.G.; Camps, M.G.M.; Li, T.M.W.Y.; Chan, A.B.; Ossendorp, F.; Cruz, L.J. Co-delivery of immunomodulators in biodegradable nanoparticles improves therapeutic efficacy of cancer vaccines. *Biomaterials* **2019**, *220*, 119417. [[CrossRef](#)] [[PubMed](#)]
24. Da Silva, C.G.; Camps, M.G.M.; Li, T.M.W.Y.; Zerrillo, L.; Löwik, C.W.; Ossendorp, F.; Cruz, L.J. Effective chemoimmunotherapy by co-delivery of doxorubicin and immune adjuvants in biodegradable nanoparticles. *Theranostics* **2019**, *9*, 6485–6500. [[CrossRef](#)]
25. Jarak, I.; Pereira-Silva, M.; Santos, A.C.; Veiga, F.; Cabral, H.; Figueiras, A. Multifunctional polymeric micelle-based nucleic acid delivery: Current advances and future perspectives. *Appl. Mater. Today* **2021**, *25*, 101217. [[CrossRef](#)]
26. Cruz, L.J.; Tacke, P.J.; Eich, C.; Rueda, F.; Torensma, R.; Figdor, C.G. Controlled release of antigen and Toll-like receptor ligands from PLGA nanoparticles enhances immunogenicity. *Nanomedicine* **2017**, *12*, 491–510. [[CrossRef](#)]
27. Duan, P.; Yanai, N.; Kimizuka, N. Photon Upconverting Liquids: Matrix-Free Molecular Upconversion Systems Functioning in Air. *J. Am. Chem. Soc.* **2013**, *135*, 19056–19059. [[CrossRef](#)]
28. Duan, P.; Yanai, N.; Nagatomi, H.; Kimizuka, N. Photon Upconversion in Supramolecular Gel Matrixes: Spontaneous Accumulation of Light-Harvesting Donor–Acceptor Arrays in Nanofibers and Acquired Air Stability. *J. Am. Chem. Soc.* **2015**, *137*, 1887–1894. [[CrossRef](#)]
29. Pilkington, E.H.; Suys, E.J.A.; Trevaskis, N.L.; Wheatley, A.K.; Zukancic, D.; Algarni, A.; Al-Wassiti, H.; Davis, T.P.; Pouton, C.W.; Kent, S.J.; et al. From influenza to COVID-19: Lipid nanoparticle mRNA vaccines at the frontiers of infectious diseases. *Acta Biomater.* **2021**, *131*, 16–40. [[CrossRef](#)]
30. Dzebo, D.; Moth-Poulsen, K.; Albinsson, B. Robust triplet–triplet annihilation photon upconversion by efficient oxygen scavenging. *Photochem. Photobiol. Sci.* **2017**, *16*, 1327–1334. [[CrossRef](#)]
31. Bansal, A.K.; Holzer, W.; Penzkofer, A.; Tsuboi, T. Absorption and emission spectroscopic characterization of platinum-octaethylporphyrin (PtOEP). *Chem. Phys.* **2006**, *330*, 118–129. [[CrossRef](#)]
32. Zuckerman, J.E.; Choi, C.H.J.; Han, H.; Davis, M.E. Polycation-siRNA nanoparticles can disassemble at the kidney glomerular basement membrane. *Proc. Natl. Acad. Sci. USA* **2012**, *109*, 3137–3142. [[CrossRef](#)] [[PubMed](#)]
33. Bae, Y.H.; Park, K. Targeted drug delivery to tumors: Myths, reality and possibility. *J. Control. Release* **2011**, *153*, 198–205. [[CrossRef](#)]
34. Jeevanandam, J.; Barhoum, A.; Chan, Y.S.; Dufresne, A.; Danquah, M.K. Review on nanoparticles and nanostructured materials: History, sources, toxicity and regulations. *Beilstein J. Nanotechnol.* **2018**, *9*, 1050–1074. [[CrossRef](#)] [[PubMed](#)]
35. Aulin, Y.V.; van Seville, M.; Moes, M.; Grozema, F.C. Photochemical upconversion in metal-based octaethyl porphyrin-diphenylanthracene systems. *RSC Adv.* **2015**, *5*, 107896–107903. [[CrossRef](#)]
36. Li, X.; Tang, Y.; Xu, L.; Kong, X.; Zhang, L.; Chang, Y.; Zhao, H.; Zhang, H.; Liu, X. Dependence between cytotoxicity and dynamic subcellular localization of up-conversion nanoparticles with different surface charges. *RSC Adv.* **2017**, *7*, 33502–33509. [[CrossRef](#)]
37. Haase, M.; Schäfer, H. Upconverting Nanoparticles. *Angew. Chem. Int. Ed.* **2011**, *50*, 5808–5829. [[CrossRef](#)]
38. Schmidt, T.W.; Castellano, F.N. Photochemical Upconversion: The Primacy of Kinetics. *J. Phys. Chem. Lett.* **2014**, *5*, 4062–4072. [[CrossRef](#)]
39. Ogawa, T.; Yanai, N.; Monguzzi, A.; Kimizuka, N. Highly Efficient Photon Upconversion in Self-Assembled Light-Harvesting Molecular Systems. *Sci. Rep.* **2015**, *5*, 10882. [[CrossRef](#)]
40. Cruz, L.J.; van Dijk, T.; Vepris, O.; Li, T.; Schomann, T.; Baldazzi, F.; Kurita, R.; Nakamura, Y.; Grosveld, F.; Philipsen, S.; et al. PLGA-Nanoparticles for Intracellular Delivery of the CRISPR-Complex to Elevate Fetal Globin Expression in Erythroid Cells. *Biomaterials* **2021**, *268*, 120580. [[CrossRef](#)]

41. Kalyane, D.; Raval, N.; Maheshwari, R.; Tambe, V.; Kalia, K.; Tekade, R.K. Employment of enhanced permeability and retention effect (EPR): Nanoparticle-based precision tools for targeting of therapeutic and diagnostic agent in cancer. *Mater. Sci. Eng. C* **2019**, *98*, 1252–1276. [[CrossRef](#)] [[PubMed](#)]
42. Hashizume, H.; Baluk, P.; Morikawa, S.; McLean, J.W.; Thurston, G.; Roberge, S.; Jain, R.K.; McDonald, D.M. Openings between Defective Endothelial Cells Explain Tumor Vessel Leakiness. *Am. J. Pathol.* **2000**, *156*, 1363–1380. [[CrossRef](#)]